*Article*

# Eutectoid Transformation Kinetics of FeO under N₂ and Air Atmospheres

Hao Wang, Guangming Cao *, Silin Li, Wencong Zhao and Zhenyu Liu

State Key Laboratory of Rolling and Automation, Northeastern University, Shenyang 110819, China
* Correspondence: caogm@ral.neu.edu.cn

**Abstract:** The effect of different oxygen content on eutectoid transformation kinetics in FeO were studied in this paper. Thermogravimetric analysis was employed to investigate the eutectoid reaction in the oxide formed on pure Fe after being exposed to air at 900 °C for 10 min. The oxidized specimens were held isothermally in $N_2$ and air from 100 s to 10,000 s in the temperature range of 350 to 550 °C, and the morphologies in FeO were observed by electron probe microanalysis. The results of the eutectoid transformation are statistically analyzed, and the dynamic model of the FeO eutectoid transformation is established based on the Johnson-Mehl-Avrami-Kolmogorov equation. Combined with the measured values and the calculation results, the time of eutectoid reaction in air is earlier than that in $N_2$. Under the experimental conditions, the formation of $Fe_3O_4$ seams can occur at the interface of the FeO-substrate after the eutectoid reaction has begun, which means the eutectoid reaction is more determined by local ion concentration changes. At the $Fe_3O_4$-FeO interface, there is a high concentration enrichment of Fe ions, giving priority to the formation of Fe-rich FeO, which makes the eutectoid phase transition time earlier than in $N_2$ conditions.

**Keywords:** oxide scale; FeO eutectoid transformation; oxygen content; $Fe_3O_4$ seam

## 1. Introduction

During the hot rolling process, an Fe-oxide scale forms on the surface of the strip. In the subsequent cooling process, the interior of the oxide scale undergoes phase transformation as the temperature decreases, and oxide scale structures with different structures are finally obtained [1]. The transformation into FeO is an important factor affecting the scale structure at room temperature [2,3]. The phase transformation process determines the subsequent processing properties of the steel and has a decisive impact on the stamping resistance, pickling behavior, and atmospheric corrosion resistance of the strip surface [4–6], so that controlling the phase transformation behavior of the oxide layer is crucial to improving the steel quality [7,8].

Many factors can affect the phase transformation in the oxide scale, such as the temperature [9], alloy elements [10,11], the growth environment of the oxide layer, and the residual stress [12] in the oxide scale. In this regard, many scholars have also conducted a large number of experimental studies and discussed the phase transition mechanism in various situations. Shigenari Hayashi [13,14] conducted an in-depth study on the eutectoid transformation behavior of pure Fe and believed that the eutectoid reaction was mainly based on (1) growth of the outer $Fe_3O_4$ layer and/or precipitation of $Fe_3O_4$, (2) formation of the $Fe_3O_4$ Seam, and (3) the eutectoid reaction in FeO. For the formation of the $Fe_3O_4$ Seam layer, Yuta Shizukawa [15] founded that the formation of the $Fe_3O_4$ Seam layer at the FeO-Substrate interface may be due to the low activation energy of Fe precipitation. Compared with the oxidation experiments of Fe-Au alloys, it was confirmed that the inward diffusion layer of Fe through the FeO/Fe interface promotes the occurrence of the eutectoid reaction. In terms of the effect of alloying elements, Suzue Yoneda [16] analyzed the effect of the Mn element with eutectoid transformation. He found that a 2 wt.% Mn addition

in the Fe substrate can delay the proeutectoid and eutectoid transformations significantly. Zhi-feng Li [17] et al. compared the oxidation behavior in dry and wet air. Voids were formed in the oxide scale under wet air, and the pores fixed the gap between the new phase and the original phase, and grain boundaries inhibit the growth of new phases. Shigenari Hayashi et al. [12] used in situ high temperature X-ray diffraction to measure the stress development of oxide scales formed from pure iron. The results showed that the isothermal transformation leads to the compressive stress of $Fe_3O_4$ and Fe in the isothermal structure. This compressive stress was relaxed in the isothermal heat treatment after the homogeneous reaction.

In the actual production of hot-rolled steel strips, the phase transition environment during cooling after coiling is quite different. As shown in Figure 1, the strip produced has visible color differences at the edge and center because of the difference in oxide scale structure. At the edge position and the outermost ring of the strip coil after coiling, it is still in the external environment and can be in direct contact with air, while the center position is in a relatively oxygen-poor environment. This difference is more pronounced when the thickness specification of the steel strip is less than 6 mm. In addition to the difference in cooling rate caused by different coil positions, the phase transition environment may also affect the process of eutectoid reaction.
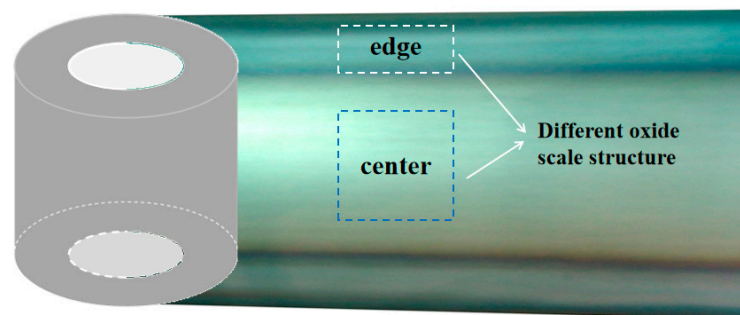


**Figure 1.** Visible color differences at the edge/center.

In this paper, pure-Fe oxide scale was used as the raw experimental material, and the different atmospheric environments (Air/$N_2$) for different durations of isothermal transformation processes were used to simulate normal oxygen content and extreme low oxygen content. The influence of the atmosphere was analyzed, and the role and mechanism of oxygen in the environment in phase transition behavior were clarified.

## 2. Experimental Procedure

Samples with dimensions of 10 mm × 8 mm × 2 mm were cut from high-purity Fe sheets (>99.99%) and normalized under vacuum at 920 °C for 20 min to remove strain and elongated grain structure. The samples were ground on silicon carbide abrasion paper to 1500 grit and then ultrasonically cleaned with acetone before oxidation and isothermal transformation tests.

Experiments were performed using a SETARAM thermal gravimetric analyzer (KEP Technologies, Lyon, France). The heating process is shown in Figure 2. The sample was first placed in the furnace chamber of the apparatus and evacuated, and then $N_2$ was introduced into it at standard atmospheric pressure. The sample was raised to 900 °C with a heating rate of 60 °C/min, and then passed through air at a rate of 100 mL/min for 10 min before being cooled to the set holding temperature (350–550 °C at a rate of 60 °C/min) and kept warm. The holding time was set to (100/500/1000/5000/10,000 s) and then cooled to room temperature at a rate of 60 °C/min.
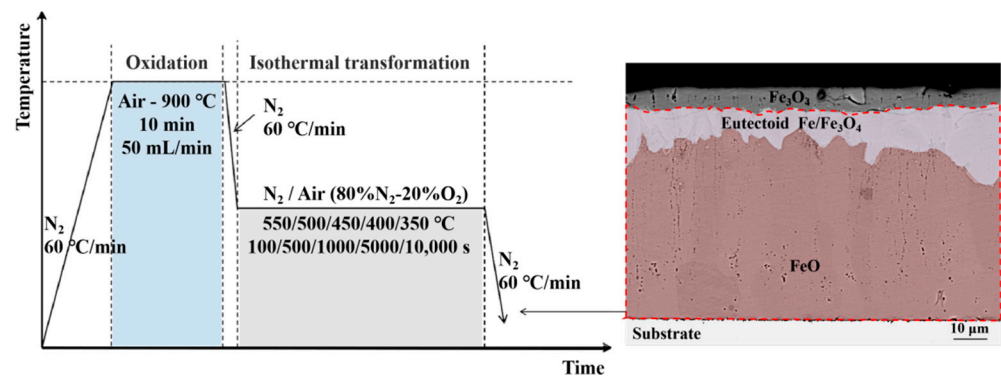
**Figure 2.** Experimental process.

The cross-sections of the samples after the experiment were mounted and then ground to 1500 grit along the direction of the oxide scale. Polishing was performed using a mechanical polisher at a rate of 500 rpm/min, and the section was etched with hydrochloric acid and alcohol. The cross-section of the corroded sample was detected and analyzed using the backscattering mode of the JXA-8530F electron probe microanalysis (EPMA) (JEOL Ltd., Tokyo, Japan). The proportion of eutectoid structure under each atmosphere and temperature (the white area marked with eutectoid $Fe/Fe_3O_4$ in Figure 2) in FeO (the area indicated by the red dotted line) was calculated.

## 3. Experiment Results

Figure 3 shows the oxide structure obtained by isothermal operation in air and an $N_2$ environment at 550 °C. In the $N_2$ atmosphere, the oxides formed in 100–10,000 s are mainly outer $Fe_3O_4$ and inner FeO. At the same time, a small amount of diamond-shaped proeutectoid $Fe_3O_4$ appears in the interior of FeO. The size of the proeutectoid $Fe_3O_4$ increases obviously, and FeO has no eutectoid structure. Under the condition that air is isothermal, the oxides formed are similar to the results of phase transformation in an $N_2$ atmosphere; the difference is that the proportion of the outer $Fe_3O_4$ layer increases during the phase transformation in air.
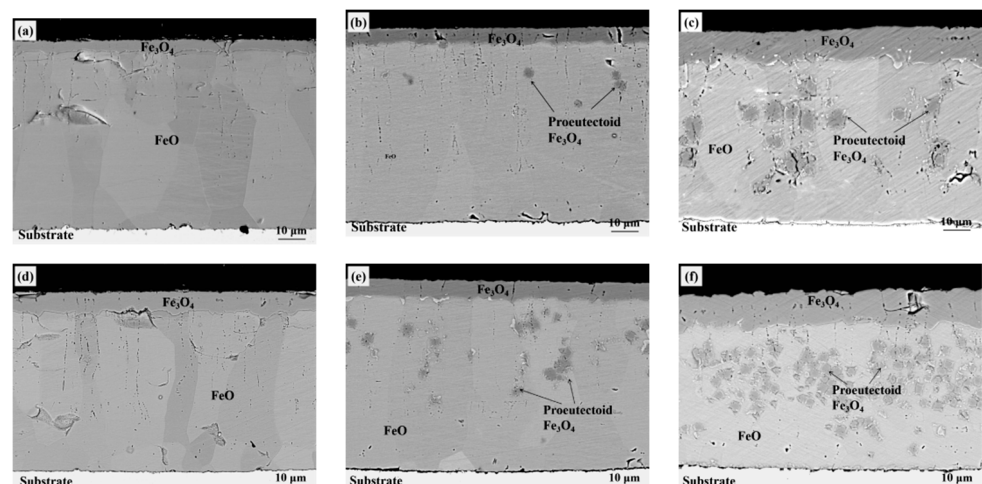


**Figure 3.** Oxidized structures under different isothermal conditions at 550 °C in an air and $N_2$ environment. (**a**) air—100 s; (**b**) air—1000 s; (**c**) air—10,000 s; (**d**) $N_2$—100 s; (**e**) $N_2$—1000 s; (**f**) $N_2$—10,000 s.

Figure 4 shows the oxide structures obtained under different isothermal conditions at 500 °C in air and $N_2$ environments. When isothermal in air for 500 s, the eutectoid structure has already formed at the $Fe_3O_4$-FeO interface, while in the $N_2$ environment, it is composed of $Fe_3O_4$ and FeO before 500 s, and the eutectoid structure will not appear

until the isothermal temperature reaches 1000 s. With the extension of isothermal time, the eutectoid structure continued to grow into the oxide scale. When times are exposed for 10,000 s, the proportion of eutectoid transformation reaches more than 85% in air and 60% in $N_2$.
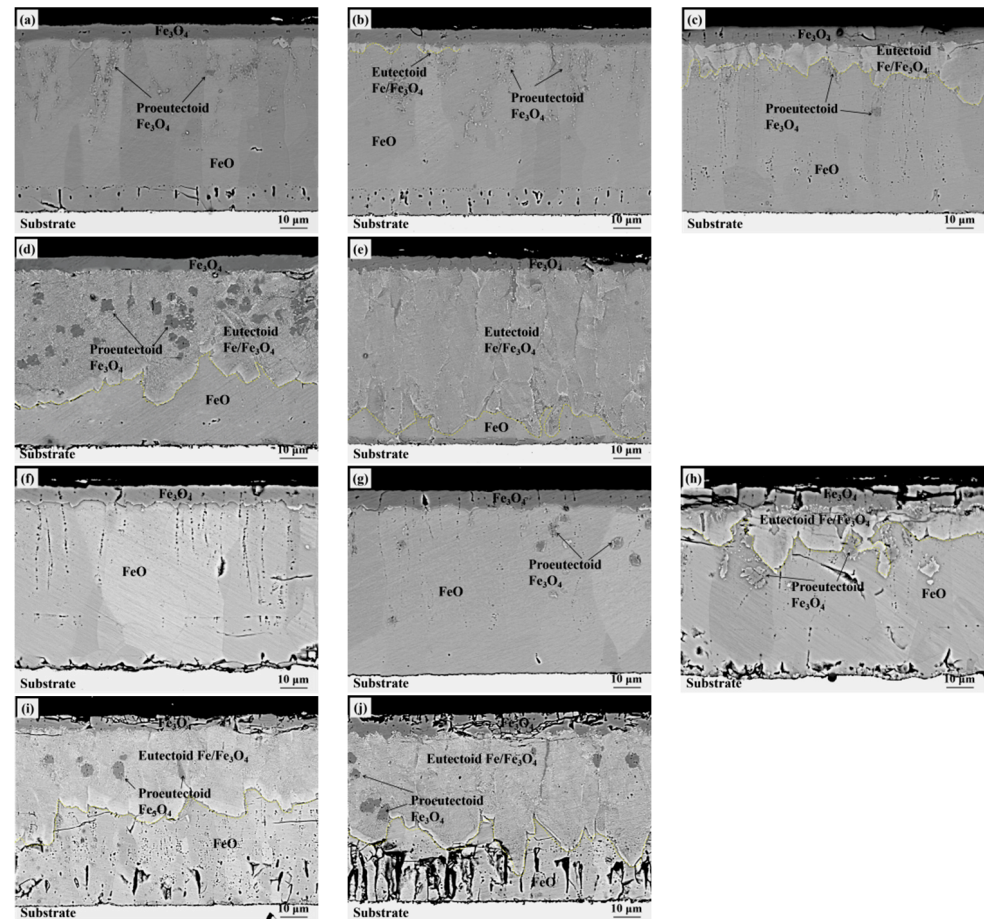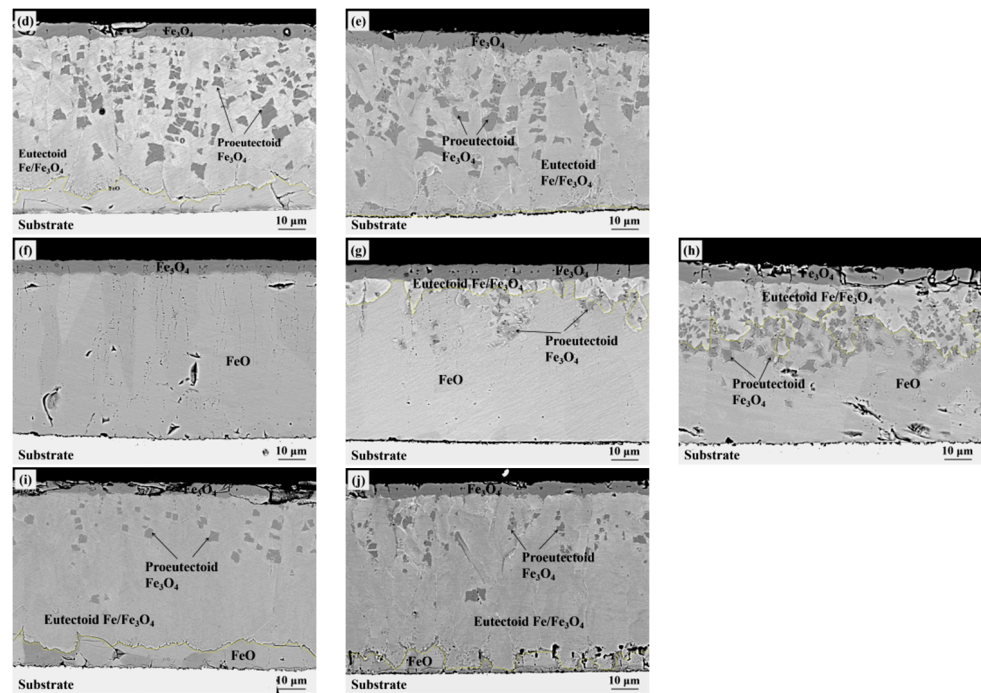


**Figure 4.** Oxidized structures under different isothermal conditions at 500 °C in an air and $N_2$ environment. (**a**) air—100 s; (**b**) air—500 s; (**c**) air—1000 s; (**d**) air—5000 s; (**e**) air—10,000 s; (**f**) $N_2$—100 s; (**g**) $N_2$—500 s; (**h**) $N_2$—1000 s; (**i**) $N_2$—5000 s; (**j**) $N_2$—10,000 s.

Figure 5 shows the oxide structures obtained under different isothermal conditions at 450 °C in air and $N_2$ environments. The time of the overall eutectoid reaction in both environments was significantly earlier than that at 500 °C. Especially in the air environment, the eutectoid structure has begun to appear at the $Fe_3O_4$-FeO interface within 100 s. The eutectoid structure has also begun to appear at the $Fe_3O_4$-FeO interface after 500 s in the $N_2$ environment. The volume of eutectoid phase transition in FeO is more than 90% at 10,000 s in both air and $N_2$ environments, which indicates the transformation is complete.
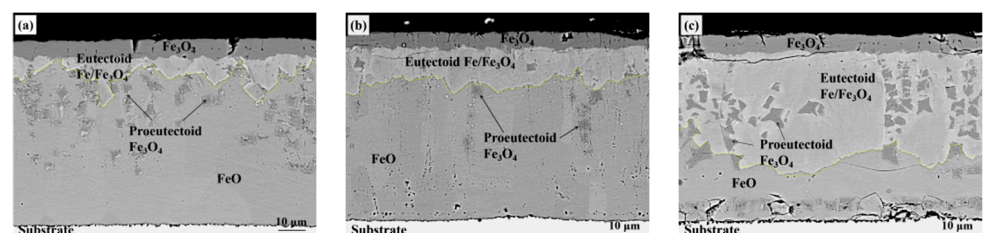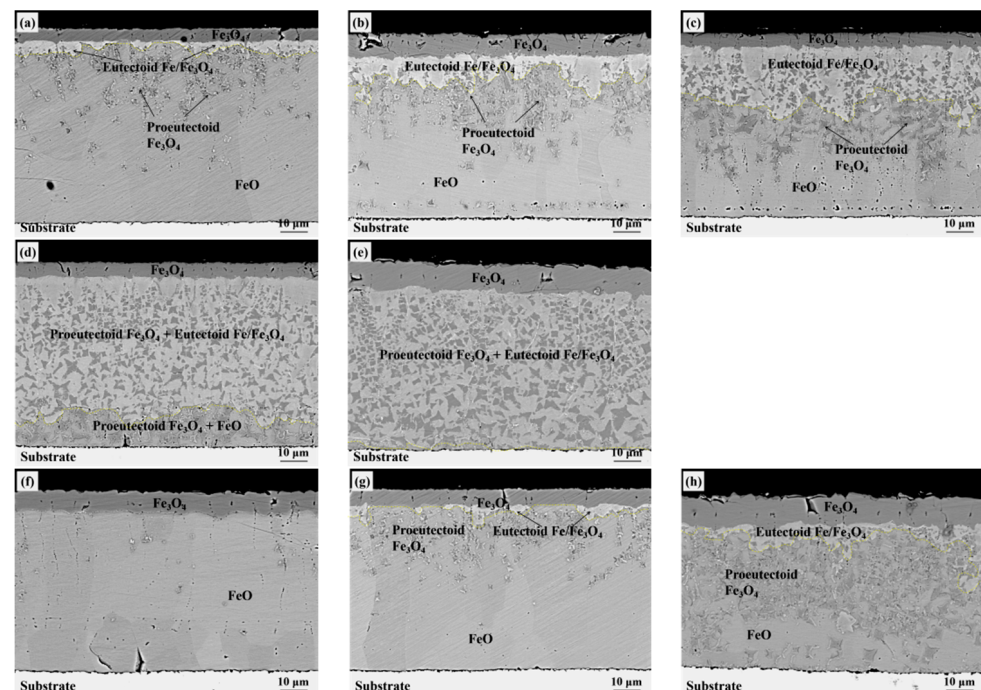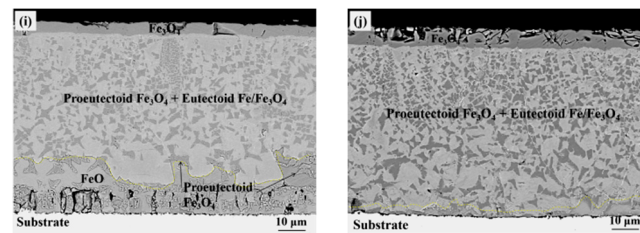


**Figure 5.** *Cont.*

**Figure 5.** Oxidized structures under different isothermal conditions at 450 °C in air and N₂ environments. (**a**) air—100 s; (**b**) air—500 s; (**c**) air—1000 s; (**d**) air—5000 s; (**e**) air—10,000 s; (**f**) N₂—100 s; (**g**) N₂—500 s; (**h**) N₂—1000 s; (**i**) N₂—5000 s; (**j**) N₂—10,000 s.

In the results of eutectoid transformation at 400 °C, shown in Figure 6, the start time of the eutectoid transformation is similar to the results at 450 °C, that is, isothermal for 100 s under air and 500 s under N₂, at which point the eutectoids at the Fe₃O₄-FeO interface have begun to appear, and at the time point when the eutectoid reaction is complete, both of them reach the complete eutectoid reaction in 10,000 s. However, the process of eutectoid reaction in air is obviously faster than that in N₂.
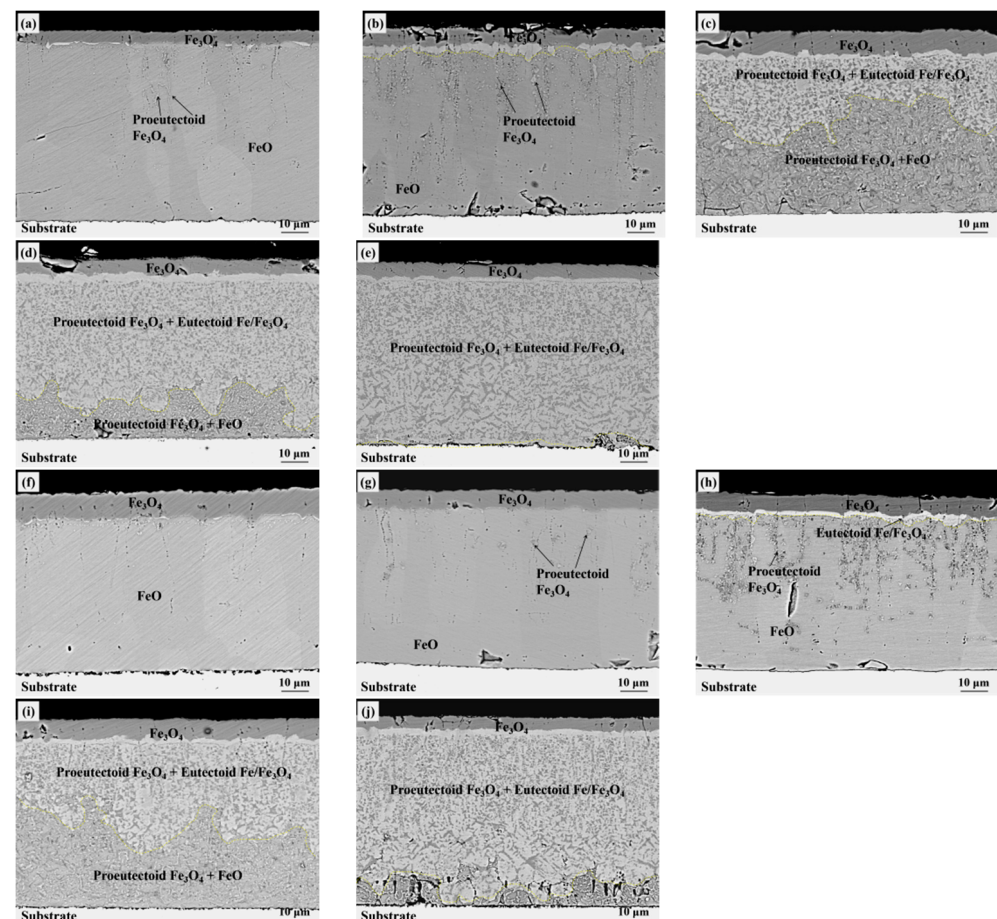


**Figure 6.** *Cont.*

**Figure 6.** Oxidized structures under different isothermal conditions at 400 °C in air and $N_2$ environments. (**a**) air—100 s; (**b**) air—500 s; (**c**) air—1000 s; (**d**) air—5000 s; (**e**) air—10,000 s; (**f**) $N_2$—100 s; (**g**) $N_2$—500 s; (**h**) $N_2$—1000 s; (**i**) $N_2$—5000 s; (**j**) $N_2$—10,000 s.

Figure 7 shows the oxide structures obtained under different isothermal times at 350 °C in air and $N_2$ environments. Different from the independent and bulky growth mode above 400 °C, at this temperature, the formed proeutectoid $Fe_3O_4$ presents a large-area small block distribution, and the eutectoid structure grows in the gaps of the proeutectoid $Fe_3O_4$. The eutectoid structure first appeared in the air at an isothermal temperature of 500 s, and the eutectoid structure did not appear until 1000 s under the $N_2$ condition. Under different conditions, both of the eutectoid phase transition processes took about 10,000 s.



**Figure 7.** Oxidized structures under different isothermal conditions at 350 °C in air and $N_2$ environments. (**a**) air—100 s; (**b**) air—500 s; (**c**) air—1000 s; (**d**) air—5000 s; (**e**) air—10,000 s; (**f**) $N_2$—100 s; (**g**) $N_2$—500 s; (**h**) $N_2$—1000 s; (**i**) $N_2$—5000 s; (**j**) $N_2$—10,000 s.

With the structural changes of the oxide scale, it can be seen that at the same temperature, proeutectoid $Fe_3O_4$ will be formed in FeO, and its nucleation quantity is related to unit volume and isothermal temperature; the eutectoid structure begins to appear at the

Fe$_3$O$_4$-FeO interface and gradually grows to the FeO-substrate interface. By comparison, two interesting phenomena occurred in this experiment. The first is the eutectoid reaction in air, which always takes priority with the N$_2$ environment at the same time. The second is that proeutectoid Fe$_3$O$_4$ is formed in FeO, and a continuous Fe$_3$O$_4$ seam layer doesn't form before the eutectoid reaction starts.

## 4. Discussion

### 4.1. Eutectoid Transformation Kinetics

The volume fraction of eutectoid structure in the FeO layer at different times when the oxidation product is isothermal at 350–500 °C was calculated, and the formation kinetic curve of eutectoid structure was obtained, as shown in Figure 8. The eutectoid transformation of FeO can be divided into two stages: the slow incubation stage and the accelerated growth stage. In the incubation stage, the eutectoid structure was found at the interface between Fe$_3$O$_4$ and FeO after isothermal heating at 400 °C and 450 °C for 100 s in an air environment, indicating that due to energy fluctuation at the interface, the eutectoid structure began to nucleate here but the eutectoid reaction did not occur at 350 °C and 500 °C. Under the condition of N$_2$, after 500 s at 400 and 450 °C, there is the eutectoid structure at the interface between outer Fe$_3$O$_4$ and FeO, and the incubation stage is significantly prolonged. In the accelerated stage after inoculation, when isothermal at 350–500 °C for 1000–10,000 s, the nucleation number of the eutectoid structure increases significantly and grows continuously. Therefore, the oxidation products undergo rapid eutectoid transformation at this stage. However, the acceleration phase time in air is relatively earlier than that in an N$_2$ environment. In addition, it can be seen from Figure 8 that the eutectoid transformation process of the steels is the most rapid when the isothermal temperature is 450 °C.
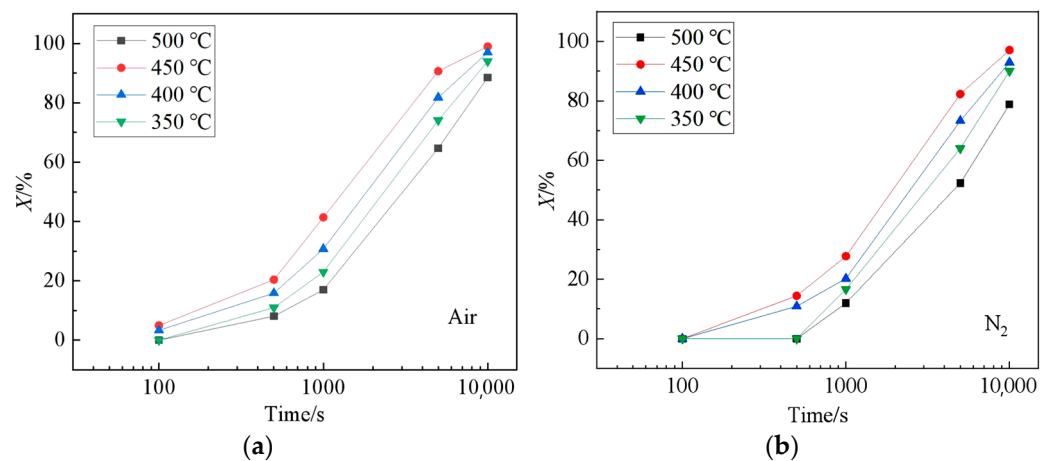


**Figure 8.** Volume fraction of eutectoid after isothermal transformation at different temperatures: (**a**) Air condition; (**b**) N$_2$ condition.

The eutectoid transformation of FeO belongs to the diffusion type of transformation, including the nucleation and growth processes. The transformation rate depends on the nucleation rate and growth rate, both of which are influenced by isothermal temperature. Therefore, the kinetics of FeO eutectoid transformation conform to the general laws of phase transformation such as nucleation and growth. The phase transformation kinetics of FeO eutectoid transformation can be described by the Johnson-Mehl-Avrami-Kolmogorov (JMAK) equation, which is a semi-empirical and semi-theoretical model to describe the isothermal phase transformation kinetics [18–20]. The variation of the volume fraction of eutectoid structure in the FeO layer with time can be expressed as:

$$X_{\text{Eutectoid}} = 1 - \exp(-Kt^n) \tag{1}$$

where $X_{eutectoid}$ is the volume fraction of the eutectoid structure in the FeO phase; t is isothermal time (seconds); $K$ is the coefficient, which depends on the phase transition temperature; and $n$ is the coefficient, depending on the type of phase transition. Equation (1) can be further transformed to obtain Equation (2):

$$\ln \ln(1/(1 - X_{Eutectoid})) = \ln K + n \ln t \tag{2}$$

The above formula shows that there is a linear relationship between lnln $(1/(1 - X_{eutectoid}))$ and ln $t$, with slope $n$ and intercept ln $K$. By substituting the statistical data of the eutectoid tissue volume fraction in the FeO layer under different isothermal conditions in Figures 4–7 into Equation (2), the fitting curve shown in Figure 9 can be obtained. The ln $k$ and $n$ values at different temperatures are shown in Table 1.
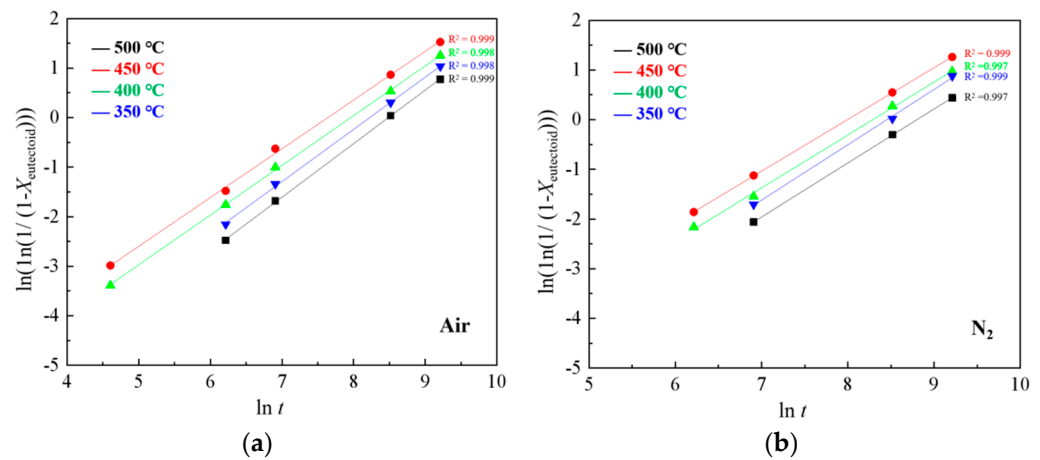


**Figure 9.** Relationship between lnln$(1/(1 - X_{Eutectoid}))$ and ln $t$: (**a**) Air condition; (**b**) $N_2$ condition.

**Table 1.** ln$K$ and $n$ at different temperature.

| Temperature /°C | Air | | | | $N_2$ | | | |
|---|---|---|---|---|---|---|---|---|
| | 500 °C | 450 °C | 400 °C | 350 °C | 500 °C | 450 °C | 400 °C | 350 °C |
| $n$ | 1.08 | 1.00 | 1.01 | 1.05 | 1.08 | 1.04 | 1.06 | 1.11 |
| ln $k$ | −9.18 | −7.69 | −7.79 | −8.87 | −9.98 | −8.50 | −8.65 | −9.68 |

The Avrami exponent $n$ in the JMAK equation depends on the type of phase transition and is independent of temperature. The value of $n$ generally varies in the range of 1–4. The $n$ values of different temperatures are averaged for subsequent calculations. Since the coefficient $k$ depends on the subcooling $\Delta T$ of the phase transition process, ln $k$ in Table 1 can be compared with $\Delta T$ to carry out the quadratic polynomial fitting, and the fitting results are shown in Figure 10 and Equations (3) and (4):

$$K(T)_{N_2} = \exp(-2.52 \times 10^{-4}T^2 + 0.3502 \times T - 129.5040) \tag{3}$$

$$K(T)_{Air} = \exp(-2.57 \times 10^{-4}T^2 + 0.3571 \times T - 131.6321) \tag{4}$$

where $k$ is the coefficient, which depends on the phase transition temperature; $T$ is the isothermal temperature (K).
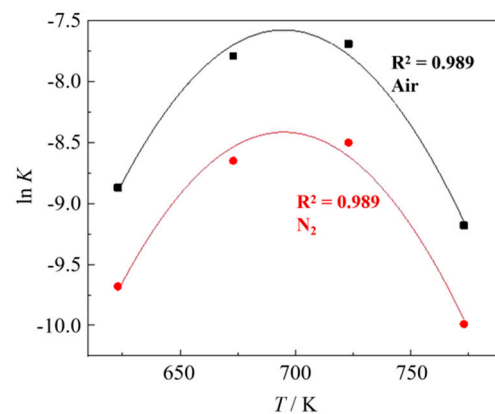
**Figure 10.** Relationship between ln *K* and *T*.

Substituting the fitting results of various parameters into the JMAK equation, the relationship between the volume fraction of eutectoid tissue in the FeO layer and time under the condition of isothermal transformation can be obtained from (5) and (6), that is,

$$X_{N_2} = (1 - \exp(-e^{(-2.52 \times 10^{-4} T^2 + 0.3502 \times T - 129.5040)} t^{1.0})) \tag{5}$$

$$X_{Air} = (1 - \exp(-e^{(-2.57 \times 10^{-4} T^2 + 0.3571 \times T - 131.6321)} t^{1.0})) \tag{6}$$

where, *X* is the volume fraction of the eutectoid structure; *T* is the isothermal temperature, K; *t* is the isothermal time (seconds). By substituting different isothermal transition temperatures *t* into Equations (5) and (6), the prediction curves of isothermal kinetic curves under different isothermal transition temperatures can be obtained. The comparison between the measured volume fraction of eutectoid structure in the FeO layer after isothermal heating at different temperatures and different times and the predicted results based on the FeO eutectoid transformation kinetic equation shown in Equations (5) and (6) is shown in Figure 10. Using Equations (5) and (6), draw the curves of eutectoid structure accounting for 5% and 95% of FeO under two different atmospheres, as shown in Figure 11. It can be seen that the eutectoid reaction process of FeO in an air environment is more advanced than that in $N_2$.
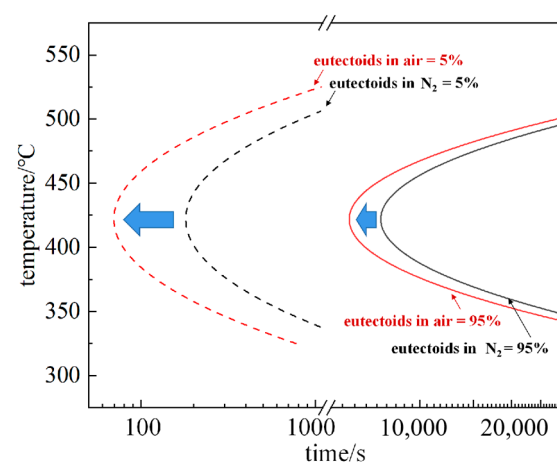


**Figure 11.** TTT diagram with calculation.

### 4.2. Oxide after High Temperature Oxidation and Fe₃O₄ Seam

Figure 12 shows the original oxide scale structure without structural transformation obtained after oxidation at 900 °C for 10 min. The thermally grown oxides consist of three iron oxides, namely hematite ($Fe_2O_3$), magnetite ($Fe_3O_4$), and wustite (FeO). Combined with the EDS and the XRD results, it can be determined that the outer layer of the oxide

scale is $Fe_2O_3$ and $Fe_3O_4$, and the inner layer is FeO, and the ratio of them is about 1:4:95. This is in good agreement with previous studies [21]. Due to the lattice disorder of $Fe_2O_3$, both iron ions and oxygen ions can diffuse in $Fe_2O_3$. After magnification, it can be seen that $Fe_2O_3$ has a honeycomb shape on the surface, which means that the components in the external atmosphere can more easily pass through $Fe_2O_3$ and continue to react with the inner Fe oxides to form Fe oxides with higher valence states. Among the three typical oxidation products, FeO, as a typical p-type semiconductor, has a wide stoichiometric form ($Fe_{0.95}O$–$Fe_{0.88}O$) and a high cation vacancy concentration [22], which improves the mobility of cations and electrons in FeO. $Fe_3O_4$ has an inverse spinel structure, and there are voids in the octahedron and the tetrahedron, so Fe ions can also diffuse rapidly in $Fe_3O_4$.
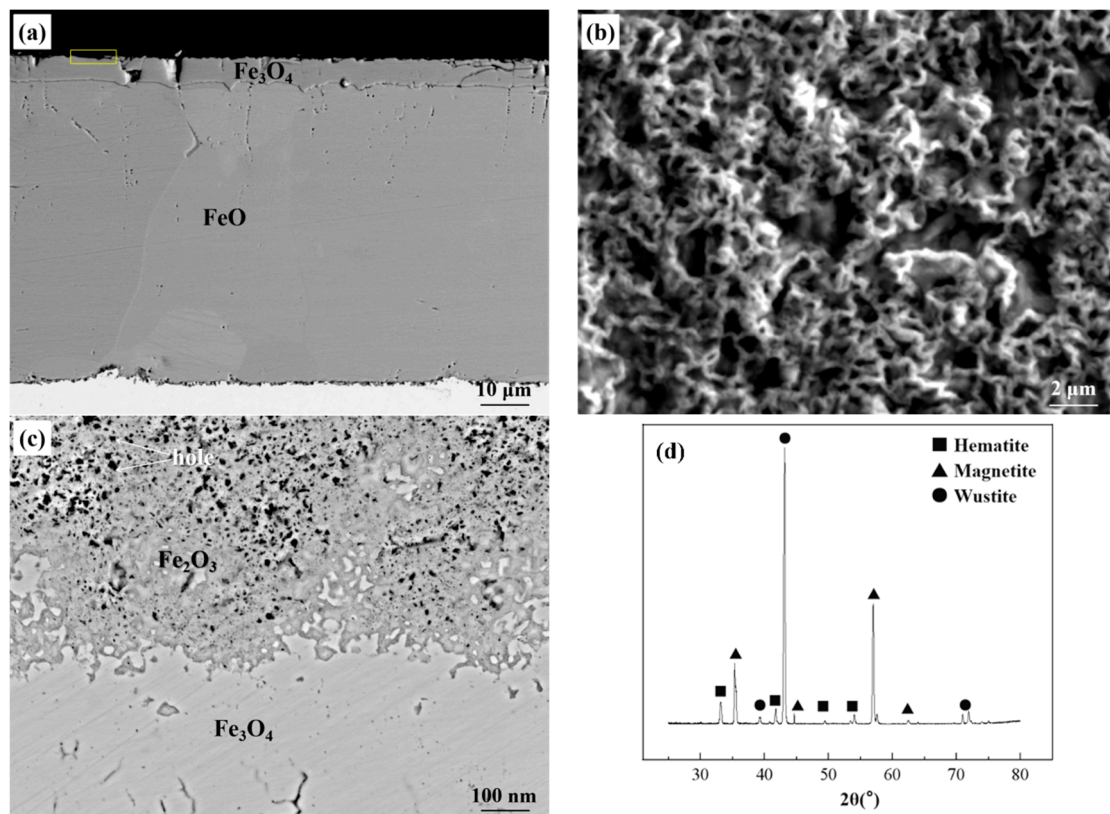


**Figure 12.** Oxide scale structure obtained after high temperature oxidation. (**a**) cross-sectional structure. (**b**) $Fe_2O_3$ with a honeycomb-like surface, and (**c**) the interface of $Fe_2O_3$-$Fe_3O_4$ obtained after local amplification in (**a**), and (**d**) the XRD results after high temperature oxidation.
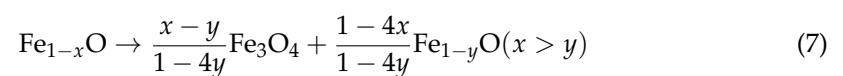
As shown in Figure 13, after the eutectoid reaction starts, $Fe_3O_4$ starts to be generated at the local position of the FeO-substrate interface. Yu [23] analyzed the formation of the $Fe_3O_4$ seam layer based on texture. According to the research results, it is assumed that there is no oxygen vacancy in pure iron oxide, and the ion radii of $Fe^{2+}$ and $Fe^{3+}$ are 0.74 Å and 0.76 Å, respectively, which are about half of the $O^{2-}$ radius. Due to the large difference in atomic size, $O^{2-}$ is easily formed into a cubic close-packed structure. In iron oxides, the mobility of oxygen anions is significantly lower than that of Fe cations without other elements because of their large ion radius and lack of oxygen vacancies. Therefore, at the FeO-substrate interface, $Fe_3O_4$ seam are always difficult to form in the experimental steel. Therefore, in this paper, the eutectoid reaction is more determined by local ion concentration changes.
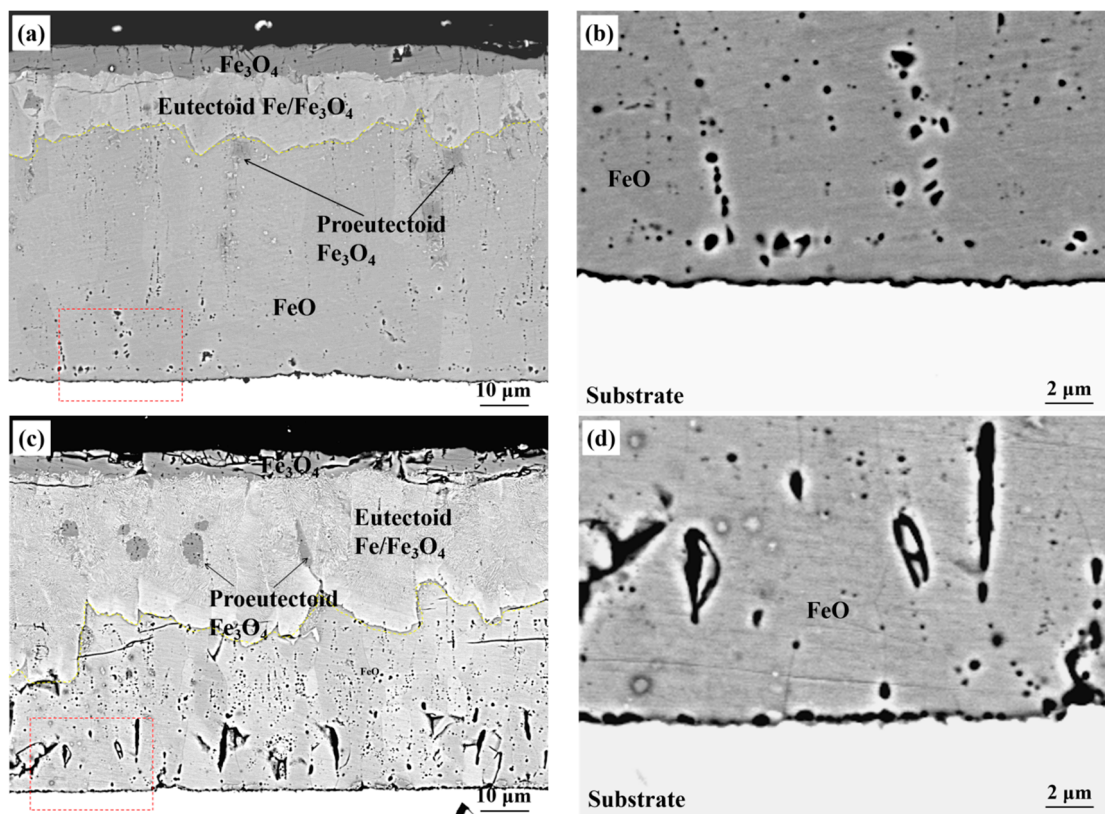
**Figure 13.** Formation of the Fe$_3$O$_4$ seam layer at the FeO-substrate interface after isothermal transformation: (**a**) air—450 °C—500 s; (**b**) magnified in the red square in (**a**); (**c**) N$_2$—500 °C—5000 s; (**d**) magnified in the red square in Figure 13c.

### 4.3. Eutectoid Transformation

FeO contains two different reaction types, namely, O-rich FeO and Fe-rich FeO. According to the Fe-O phase diagram in Figure 14, the equilibrium region of the O-rich FeO and FeO phases intersects at point d. With the decrease in temperature, the Fe$_3$O$_4$ phase with proeutectoid reactions will precipitate in FeO, and FeO will change from O-rich FeO to Fe-rich FeO. The reaction path that follows the reaction path is b→d→e/e′, which is shown in reaction (7):

$$\mathrm{Fe}_{1-x}\mathrm{O} \rightarrow \frac{x-y}{1-4y}\mathrm{Fe}_3\mathrm{O}_4 + \frac{1-4x}{1-4y}\mathrm{Fe}_{1-y}\mathrm{O}\,(x>y) \tag{7}$$

When the O-rich FeO is transformed into Fe-rich FeO through the above reaction, eutectoid transformation occurs, resulting in a lamellar eutectoid structure of Fe+Fe$_3$O$_4$ is formed:

$$4\mathrm{Fe}_{1-y}\mathrm{O} \rightarrow \mathrm{Fe}_3\mathrm{O}_4 + (1-4y)\mathrm{Fe} \tag{8}$$
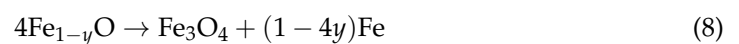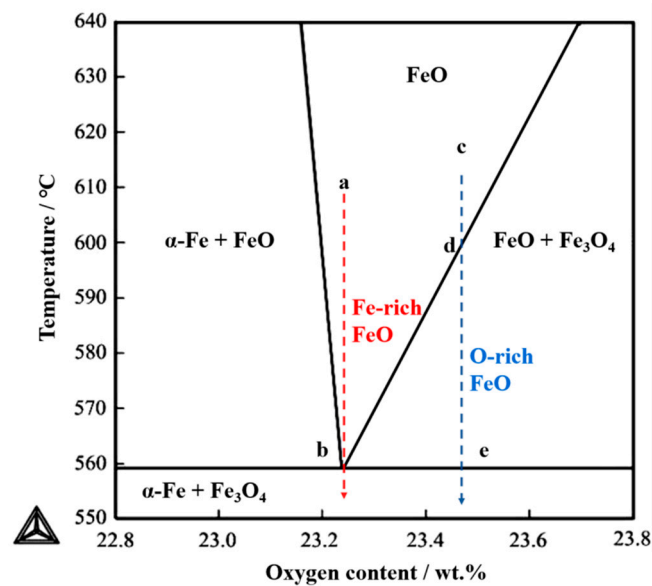
**Figure 14.** Fe-O diagram.

Therefore, whether Fe-rich FeO can be formed preferentially will determine the eutectoid reaction process. In this experiment, the content of Fe ions in FeO mainly depends on two factors:

The first factor is the reaction temperature, which can be described in two aspects: when the isothermal transformation process is carried out at a relatively high temperature (500 °C, for example). At this time, the Fe cation can always diffuse from the steel substrate to the oxide scale, resulting in an increase in the Fe ion concentration in FeO, the direct formation of relatively Fe-rich FeO, and the eutectoid reaction path closer to a→b. At this time, the eutectoid reaction can occur without the formation of a large number of proeutectoid $Fe_3O_4$ in FeO.

When the formation temperature of the eutectoid structure is relatively low (350 °C, for example), the diffusion of Fe ions into FeO through the substrate is limited, and the occurrence of O-rich FeO in the eutectoid reaction will depend more on the proeutectoid reaction to increase the Fe ion concentration in FeO. At this time, through the c→d→e path, proeutectoid $Fe_3O_4$ will nucleate in FeO, and the number of nucleations will increase significantly at any time when the temperature decreases, resulting in a large number of proeutectoid $Fe_3O_4$ occupying FeO. Due to a large amount of proeutectoid growth, the rate of eutectoid reaction in FeO did not decrease significantly at 350 °C.

The second factor is the increase in local Fe ion concentration caused by the O element in the environment. In this experiment, the effect of reaction temperature was excluded by controlling variables. Since the eutectoid temperature was above 350 °C in the whole experiment, $Fe_2O_3$ and $Fe_3O_4$ still maintained the trend of continuous growth on the outside of FeO. Because $Fe_2O_3$ is porous, O can directly contact the $Fe_3O_4$ layer and react with it so that the Fe ions in $Fe_3O_4$ are consumed. The resulting concentration gradient will be that Fe ions in FeO will enrich towards the $Fe_3O_4$-FeO interface, forming a peak concentration gradient of Fe ions at the interface. As shown in Figure 15. The Fe-rich FeO in the inner layer was formed by the depletion diffusion of the outer layer, which made the eutectoid reaction of FeO start in advance. The effects persisted until the end of the eutectoid reaction.
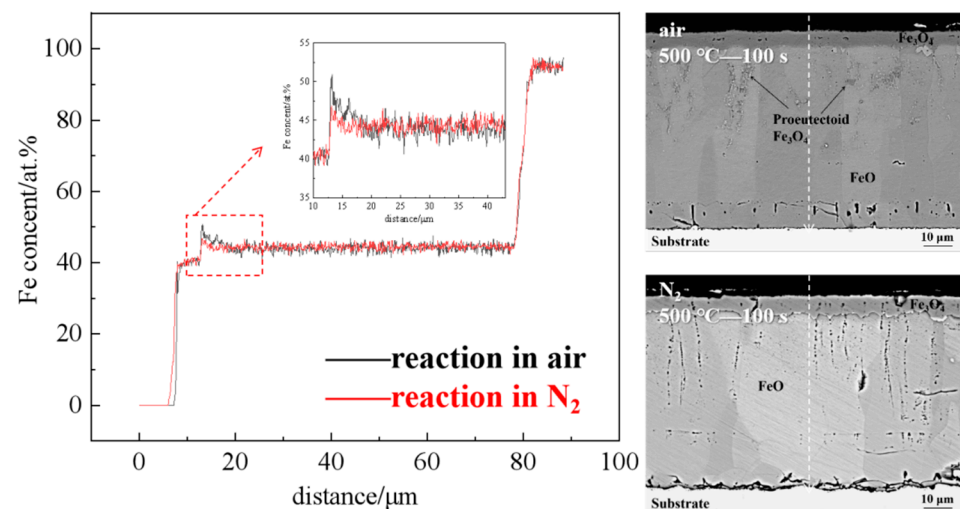
**Figure 15.** Fe element distribution at the interface in the $Fe_3O_4$-FeO before the start of the eutectoid transformation.

## 5. Conclusions

1. Model of FeO eutectoid transformation is established based on the JMAK equation, and the time of eutectoid structure in air is earlier than that of $N_2$.
2. $Fe_3O_4$ seams formed at the interface of the FeO-substrate after the eutectoid reaction began, which means they are not a necessary condition of the eutectoid reaction. The eutectoids are more affected by local ion concentration changes in this experiment.
3. The isothermal temperature affects the concentration of Fe ions in FeO, which directly determines the nucleation and growth of proeutectoid in FeO.
4. In air conditions, there is a high concentration enrichment of Fe ions at the $Fe_3O_4$-FeO interface because of the oxygen in the environment, which gives priority to the formation of Fe-rich FeO and makes the eutectoid phase transition time earlier than $N_2$ conditions.

**Author Contributions:** H.W.: conceptualization, methodology, investigation, writing—original draft, writing—review and editing. G.C.: investigation, writing—review and editing, and funding acquisition. S.L.: investigation. W.Z.: investigation and supervision. Z.L.: conceptualization, methodology, project administration, and funding acquisition. All authors have read and agreed to the published version of the manuscript.

**Data Availability Statement:** Not applicable.

## References

1. Chen, R.Y.; Yuen, W.Y.D. Oxide-Scale Structures Formed on Commercial Hot-Rolled Steel Strip and Their Formation Mechanisms. *Oxid. Met.* **2001**, *56*, 89–118. [CrossRef]
2. Gleeson, B.; Hadavi, S.M.M.; Young, D.J. Isothermal transformation behavior of thermally-grown wüstite. *Mater. High Temp.* **2000**, *17*, 311–318. [CrossRef]
3. Lin, S.N.; Hung, G.C.; Wu, M.T.; Wang, W.L.; Hsieh, K.C.S. Crucial Mechanism to the Eutectoid Transformation of Wüstite Scale on Low Carbon Steel. *Steel. Res. Int.* **2017**, *88*, 1700045. [CrossRef]
4. He, Y.Q.; Jia, T.; Li, Z.F.; Cao, G.M.; Liu, Z.Y.; Li, J. Hot-dip Galvanizing of Carbon Steel after Cold Rolling with Oxide Scale and Hydrogen Descaling. *J. Iron Steel Res. Int.* **2014**, *21*, 222–226. [CrossRef]
5. Liu, X.J.; Cao, G.M.; He, Y.Q.; Yang, M.; Liu, Z.Y. Reduction of Oxide Scale with Hydrogen. *J. Iron Steel Res. Int.* **2014**, *21*, 24–29. [CrossRef]

6.    Li, Z.F.; He, Y.Q.; Cao, G.M.; Tang, J.J.; Zhang, X.J.; Liu, Z.Y. Effects of Al contents on microstructure and properties of hot-dip Zn-Al alloy coatings on hydrogen reduced hot-rolled steel without acid pickling. *J. Iron Steel Res. Int.* **2017**, *24*, 1032–1040. [CrossRef]

7.    Liu, Z.Y.; Cao, G.M. *Studies on Oxidation Behavior of Steels during Hot Rolling and Development and Application of the Scale Control Techologies*; Metallurgical Industry Press: Beijing, China, 2021.

8.    Young, D.J. *High Temperature Oxidation and Corrosion of Metals*, 2nd ed.; Elsevier: Amsterdam, The Netherlands, 2016.

9.    Tanei, H.; Kondo, Y. Effects of Initial Scale Structure on Transformation Behavior of Wüstite. *ISIJ Int.* **2012**, *52*, 105–109. [CrossRef]

10.   Li, Z.F.; Cao, G.M.; Lin, F.; Cui, C.Y.; Wang, H.; Liu, Z.Y. Phase Transformation Behavior of Oxide Scale on Plain Carbon Steel Containing 0.4 wt.% Cr during Continuous Cooling. *ISIJ Int.* **2018**, *58*, 2338–2347. [CrossRef]

11.   Takeda, M.; Kushida, H.; Onishi, T.; Toyama, M.; Koizumi, F.; Fujimoto, S. Influence of Oxidation Temperature and Cr Content on the Adhesion and Microstructure of Scale on Low Cr Steels. *Oxid. Met.* **2010**, *73*, 1–13. [CrossRef]

12.   Hayashi, S.; Yamanouchi, Y.; Hayashi, K.; Hidaka, Y.; Sato, M. Stress measurement in the iron oxide scale formed on pure Fe during isothermal transformation by in situ high-temperature X-ray diffraction. *Cor. Sci.* **2021**, *187*, 109482. [CrossRef]

13.   Hayashi, S.; Mizumoto, K.; Yoneda, S.; Kondo, Y.; Tanei, H.; Ukai, S. The Mechanism of Phase Transformation in Thermally-Grown FeO Scale Formed on Pure-Fe in Air. *Oxid. Met.* **2014**, *81*, 357–371. [CrossRef]

14.   Hayashi, S.; Yoneda, S.; Kondo, Y.; Tanei, H. Phase Transformation of Thermally Grown FeO Formed on High-Purity Fe at Low Oxygen Potential. *Oxid. Met.* **2020**, *94*, 81–93. [CrossRef]

15.   Shizukawa, Y.; Hayashi, S.; Yoneda, S.; Kondo, Y.; Tanei, H.; Ukai, S. Mechanism of Magnetite Seam Formation and its Role for FeO Scale Transformation. *Oxid. Met.* **2016**, *86*, 315–326. [CrossRef]

16.   Yoneda, S.; Hayashi, S.; Kondo, Y.; Tanei, H.; Ukai, S. Effect of Mn on Isothermal Transformation of Thermally Grown FeO Scale Formed on Fe–Mn Alloys. *Oxid. Met.* **2017**, *87*, 125–138. [CrossRef]

17.   Li, Z.F.; Cao, G.M.; Lin, F.; Wang, H.; Liu, Z.Y. Characterization of Oxide Scales Formed on Plain Carbon Steels in Dry and Wet Atmospheres and Their Eutectoid Transformation from FeO in Inert Atmosphere. *Oxid. Met.* **2018**, *90*, 337–354. [CrossRef]

18.   Johnson, W.A.; Mehl, R.F. Reaction kinetics in process of nucleation and growth. *Trans. Am. Inst. Min. Metall. Eng.* **1939**, *135*, 416–458.

19.   Avrami, M. Kinetics of phase change I. General theory. *J. Chem. Phys.* **1939**, *7*, 1103–1112. [CrossRef]

20.   Kolmogorov, A.N. On the statistical theory of metal crystallization. *Bull. Acad. Sci. USSR* **1937**, *3*, 355–359. [CrossRef]

21.   Schwenk, W.; Rahmel, A. Theoretical considerations on phase boundary reactions and mass transfer during the oxidation of iron. *Oxid. Met.* **1986**, *25*, 293–303. [CrossRef]

22.   Engell, H.; Eisenhuttenwesen, J. Untersuchungen über Thermodynamik und Zusammensetzung des Wüstits. *Arch. Eisenhütten-wesen* **1957**, *28*, 109–115. [CrossRef]

23.   Yu, X.L.; Jiang, Z.Y.; Zhao, J.W.; Wei, D.B.; Zhou, C.L.; Huang, Q.X. Microstructure and microtexture evolutions of deformed oxide layers on a hot-rolled microalloyed steel. *Cor. Sci.* **2015**, *90*, 140–152. [CrossRef]